Annals of Biomedical Engineering, Vol. 22, pp. 229–239, 1994
Printed in the USA.

0090-6964/94 $10.50 + .00

Measurement of the Geometric Parameters of the Aortic Bifurcation from Magnetic Resonance Images

HONG SUN, BARRY D. KUBAN, PETRA SCHMALBROCK, AND MORTON H. FRIEDMAN

Biomedical Engineering Center and Department of Radiology, The Ohio State University, Columbus, OH

Abstract—This paper presents a method for measuring arterial geometry *in vivo* using MRI. The approach was validated using MR images of three perfused compliant casts of human aortic bifurcations whose geometry was known. Preliminary human studies demonstrated the reproducibility of the technique. The approach was applied to 20 normal individuals to study the effects of age, race, and gender on the geometry of the aortic bifurcation. The results show that older people tend to have a smaller bifurcation angle, lower planarity, and larger angular asymmetry than younger people. Asians have larger bifurcation angles than whites. The bifurcation of males is more asymmetric than that of females. These results may have implications regarding the heritability of arterial geometry, the similarities of cardiovascular risk within families, and differences in risk among groups.

Keywords—MRI, Abdominal aorta, Geometry, Aortic bifurcation, Branch angle.

INTRODUCTION

The geometry of the arteries at or near arterial bifurcations influences the blood flow field, which is an important factor affecting atherogenesis. Thus an individual's unique arterial geometry might influence that person's risk of arterial disease (8,10,21,24). The ability to measure arterial geometry *in vivo* would be useful for testing this hypothesis, and for screening purposes should it be found to be valid.

Among the possibly important geometric parameters at a branch are the angles between the vessels. Branch angles have been estimated from *in vivo* angiograms obtained radiographically. Fanucci *et al.* (6) used angiography to evaluate the branching characteristics of human arterial bifurcations. Lee (16) measured the angle between the iliac vessels at the human aortic bifurcation from aortograms using a protractor. Saltissi *et al.* (23) also used a protractor to measure the bifurcation angle between the left anterior descending and left circumflex arteries from *in vivo* coronary angiograms. All of these investigators measured the bifurcation angle in a single projection, which could not be guaranteed to be parallel to the plane of the bifurcation. Three-dimensional quantitative coronary angiography techniques provide a 3-D representation of the coronary arteries using two angiograms acquired at different projection angles. Vessel axes in 3-space can be derived by thinning the artery images in pairs of vascular angiograms and pairing points from the two projections (11). The bifurcation angle can then be calculated from straight line approximations to relatively short vessel axis segments. This approach avoids errors that accompany the use of a single projection which may not be precisely in the ''plane'' of the bifurcation.

When X-ray angiography is used, patients are injected with an intravascular contrast dye and exposed to ionizing radiation. The technique is invasive and can be harmful. Therefore, it is desirable to find a noninvasive method for accurate *in vivo* measurement of vessel geometry in three-dimensional (3-D) space. Here, we examine the ability of magnetic resonance imaging (MRI) to measure arterial geometry in living subjects.

In MRI, the displacement of flowing blood within a spatially varying magnetic field provides inherent contrast between the blood and stationary tissue (26). MR images of arteries and veins can therefore be obtained without injecting intravascular contrast agents (17). The availability of flow-compensated 3-D gradient-echo pulse sequences has enabled us to acquire MR angiography data with good contrast between the lumen and surrounding tissue (3,5,14,25,27). Because the abdominal aorta is large and important anatomically and physiologically, much early magnetic resonance imaging work was done with this vessel. Various pathological lesions of the aorta have been evaluated with MRI (19). Jackson *et al.* (12) developed an algorithm to segment the aorta automatically from transverse MR images with the goal of noninvasively evaluating the progression of atherosclerosis. Several researchers are producing 3-D views of vascular structures based on MRI data (7,13,20,22,28,29).

Acknowledgment—This research was supported by NIH (Grant HL42302), AHA-Ohio Affiliate (Grant C-92-16-S), and The Whitaker Foundation.

Address correspondence to Dr. Morton H. Friedman, Biomedical Engineering Center, The Ohio State University, 270 Bevis Hall, 1080 Carmack Road, Columbus, OH 43210.

(Received 27Aug93, Revised 21Dec93, Accepted 12Jan94)

This paper presents a method for visualizing human vascular structures and evaluating their geometry quantitatively from axial images obtained by MRI. The geometric parameters selected to evaluate the technique are the angles at the aortic bifurcation of man. A computer modeling approach is employed to display the abdominal aorta and to measure the angles at the bifurcation. The algorithms were validated using three replicas of human aortic bifurcations obtained at autopsy. After preliminary human studies demonstrated the reproducibility of the technique, the approach was applied to 20 normal individuals to study the effects of age, race, and gender on the geometry of the aortic bifurcation. A portion of this work was presented earlier at the 1991 ASME Biomechanics Symposium (9).

METHODS

The first part of this research was carried out to assess the ability of MRI to provide vascular geometric information by comparing the 3-D Time-of-Flight (3-D TOF) MR images of three compliant replicas of human aortic bifurcations against their known "gold standard" geometries. Next, the reproducibility of the MRI technique was tested by performing a series of *in vivo* measurements of the bifurcation angles and planarities of the abdominal aortic bifurcation in six healthy human beings. Finally, the approach was applied to 20 healthy individuals in two age groups. The angles at the aortic bifurcation, the angular asymmetry, and the planarity of the aortic bifurcation were calculated and analyzed statistically to determine if age, gender, or race have any influence on human arterial geometry.

Validation

Compliant Cast Preparation and MR Imaging. Three compliant flow-through casts were made with Sylgard silicone rubber from luminal molds of human aortic bifurcations obtained at autopsy (15). Each cast was mounted in a clear plastic box, which was filled with water to simulate the magnet loading of a patient. No metallic parts were used. Figure 1 shows one of the casts used in this investigation. The casts were perfused with a blood analog fluid, an aqueous solution of $MnCl_2$ and Xanthan gum, which was designed to match the rheology and T1 relaxation time of human blood. A computer-controlled positive displacement pump, which was connected to the cast with flexible plastic tubing, provided a physiologically realistic flow wave (Fig. 2) in the compliant cast. The pump system included a gear pump with electronic speed control to generate the steady component of the physiologic flow and a computer-controlled bellows pump to generate the pulsatile component. The pump system was placed in a room adjacent to the magnet room and was connected to the cast by a length of plastic tubing that passed through an access hole in the wall. The working fluid was collected in a small plastic holding tank near the cast and returned to the pump system via another length of tubing.

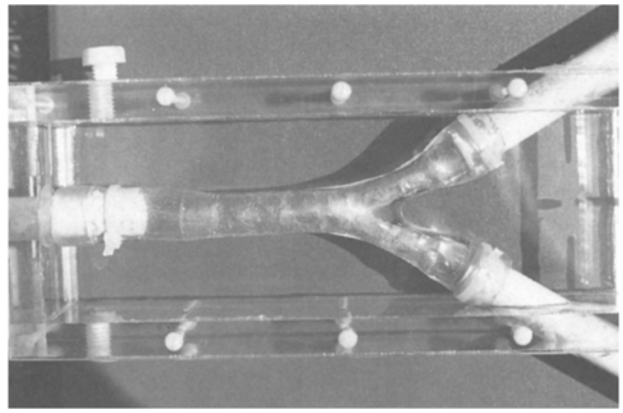

FIGURE 1. A compliant flow-through cast made with Sylgard silicone rubber from an autopsy specimen of a human aortic bifurcation.

The MRI studies were performed with a 1.5 T system (GE Signa MR System). Axial MR scans of these casts were made using a 3-D TOF angiography gradient echo pulse sequence with first-order flow compensation (14,25). Sixty cross-sectional MR images of each cast, 1.5 mm thick, were obtained from 45 mm proximal to 45 mm distal to the flow divider tip. A 256 × 128 scan matrix was applied over a 20 cm × 20 cm field of view. The images were acquired with a repetition time of 50 msec, an echo time of 7 msec and a flip angle of 15°. The scan time was about 7 min. The same 3-D TOF angiography protocols were used subsequently for the *in vivo* human studies.

"Gold Standard" Block Preparation and Video Image Acquisition. The luminal mold used to make each compliant

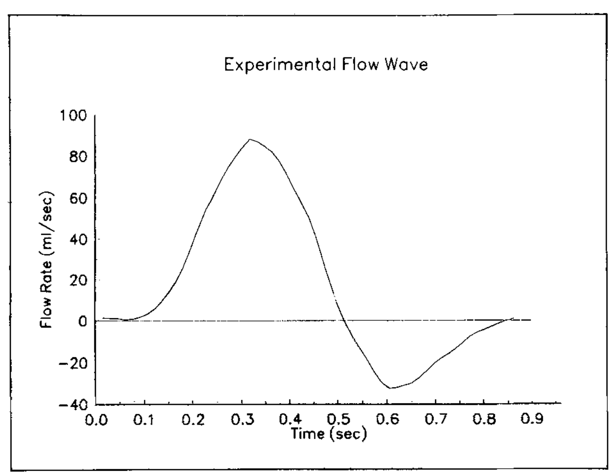

FIGURE 2. Experimental flow wave.

cast was also used to make a rigid plastic cast (termed a ''block'') which reproduced the interior shape of the vessel and served as a ''gold standard'' for comparison with the MRI data. The lumen of the block was filled with colored plastic. The plastic block was clamped to a milling machine and its surface was milled away, exposing the lumen cross-section. At 1.5-mm intervals, several seconds of video images of the milled surface were recorded on tape using a Ricoh R108-H VCR. Calibration marks on the block were imaged at the same time to obtain absolute pixel dimensions. The depth interval between video images was set at 1.5 mm to provide the same resolution in the axial direction as that of the MR data. The video images were then digitized on a VMS System with 512 × 512 spatial resolution.

Image Preprocessing and Analysis. The MR angiographic images and the video images of the ''gold standard'' block comprise two series of 2-D transverse slices. The relevant portions of the MR images and the digitized video images were transferred to a DECstation 5000/25 workstation for processing. For each set, an X Window System image processing routine was used to outline the contours of 30 cross-sectional images near the aortic bifurcation, 15 proximal and 15 distal. The contour data were then used to reconstruct the axes of the terminal aorta and the two common iliac arteries in 3-space, and to calculate the branch angles and other geometric parameters at the aortic bifurcation.

In recent years, there has been a great amount of research on automatic segmentation algorithms for tomographic data, such as edge detection, region growing, and classification methods (12). These automated segmentation techniques require very high contrast and good quality images. In MR datasets of the human trunk, the major vessels have low-contrast edges, necessitating user interaction to obtain a reliable outline of the lumen. Since the end objective of this research is an *in vivo* application, manual segmentation was used for the validation exercise, even though the luminal interface in the images of the cast was much better defined than in clinical images (Fig. 3). Segmentation was performed with an X Window System routine on the workstation, using a mouse. The image analysis reported here was all done by a single individual;

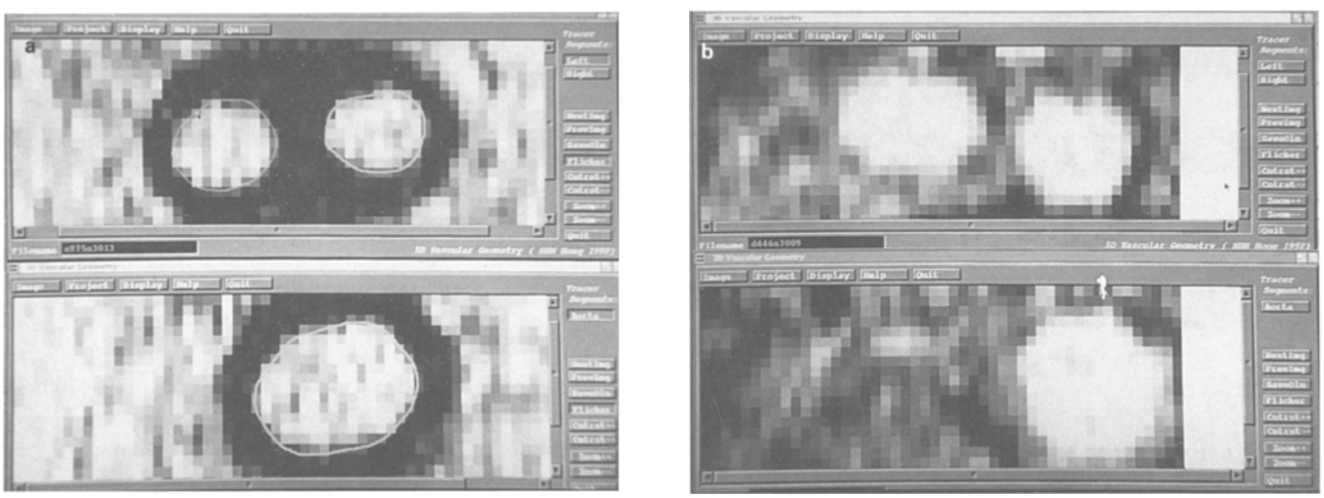

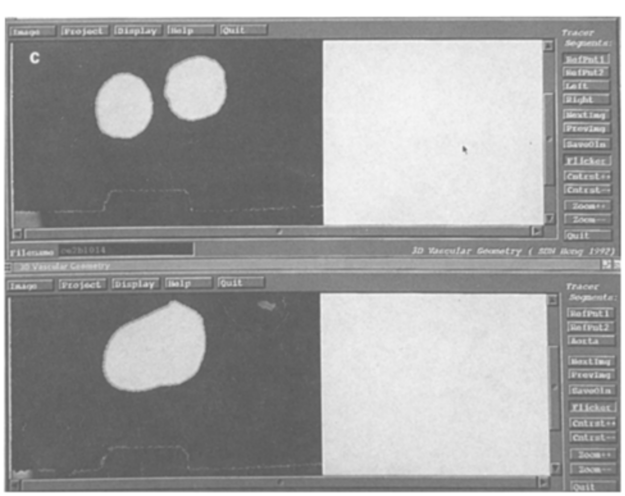

FIGURE 3. The enlarged selected regions of (a) two 3-D TOF MR images of the compliant cast, (b) the corresponding video images of the cross-section of the gold standard block at the similar levels, and (c) the *in vivo* MR images as displayed on the workstation. The video images (b) with 4 × 5 aspect ratio are stretched vertically when they are displayed with square pixels on the screen of the workstation. The edges of the vessels on (a) are outlined with the X Window System program.

interoperator variability had earlier been shown to be minimal for both the "gold standard" and MRI images.

The contours from both the MR images and the video images were used to calculate the perimeter, cross-sectional area, and shape factor of each cross-section for comparison. The shape factor is defined as $4\pi A/P^2$, where P is the perimeter and A is the cross-sectional area.

Geometric Parameter Calculation at the Aortic Bifurcation. The branch angles at the aortic bifurcation are defined as the angles between linear fits to the center lines of the three vessels in the vicinity of the junction point. Therefore, the center lines (or "vessel axes") need to be found prior to calculating the branch angles.

The vessel axes are created by connecting the centroids of the vessel cross-sections on successive slices. The vessel contours are used to calculate the centroids (xc, yc, zc). The centroid of a vessel on a 2-D image (xc, yc) is approximated by the average of all points (x, y) on the vessel contour. This is clearly an approximation that ignores the irregularity of the vessel cross-section. The error of the approximation is greatest when calculating the centroids of the few slices with concave or dumbbell-shaped vessel cross-sections near the branch point. These slices, which define the transition region *between* the parent and daughter vessels, are not used to define the vessel axes. For instance, referring to the sketch in Fig. 4, slice 6 and slice 7 are not used. The coordinate of the centroid in the z direction, zc, is determined by the position of the slice; *i.e.*, $zc = i \times d$, where i is the slice number and d is the slice thickness.

To calculate the branch angle between the iliac arteries and the two turning angles between the aorta and each daughter vessel, least-squares linear fits to the axes of the terminal aorta and the proximal portions of the two branch vessels were constructed over a length of axis equal to one vessel diameter (Fig. 4). The angle between pairs of vessels is calculated in 3-D space from the vector representations of these linear fits:

$$\cos\theta = v_1 \cdot v_2 = l1 * l2 + m1 * m2 + n1 * n2, \quad (1)$$

where $v_1 = (l1, m1, n1)$ and $v_2 = (l2, m2, n2)$ are the selected pair of unit vectors determined from the least-squares fits described above.

If the aorta and the two common iliac arteries are in the same plane at the bifurcation, the sum of the branch angles between the iliac arteries (θ_b), and the turning angles θ_{t1} and θ_{t2} should be exactly 360°. Generally, the bifurcation is not planar, and the sum of these three angles is less than 360°. Thus the "planarity" (P) of the bifurcation can be defined as the sum of the three angles divided by 360°:

$$P = (\theta_b + \theta_{t1} + \theta_{t2})/360. \quad (2)$$

The planarity is unity if the aorta and the two common iliac arteries are in the same plane at the bifurcation.

The "asymmetry" (A) of the bifurcation is defined as the absolute difference between the two turning angles, θ_{t1} and θ_{t2}:

$$A = |\theta_{t1} - \theta_{t2}|. \quad (3)$$

The bifurcation is symmetric if θ_{t1} and θ_{t2} are equal.

3-D Aorta Surface Formation and Display. The production of 3-D images from serial sections involves two steps: surface reconstruction and surface display. The surface of the bifurcation is reconstructed by triangulation of a sequence of contour outlines (4,29,30); the surface is modeled as a collection of connected triangles. This surface model may be displayed from arbitrary perspectives as a wireframe drawing or as a shaded rendering of the vessel on a raster CRT graphics device. The graphics software, "Rayshade," was used to generate smooth shading for the aorta. It reads the triangular definition of the segment and produces a Utah Raster RLE format file of the ray-traced image of the vessels. RayShade implements a ray tracing algorithm (1) in conjunction with global illumination models that account for reflection of one object on the surface of another, refraction, transparency, and shadow effects. The images are also antialiased.

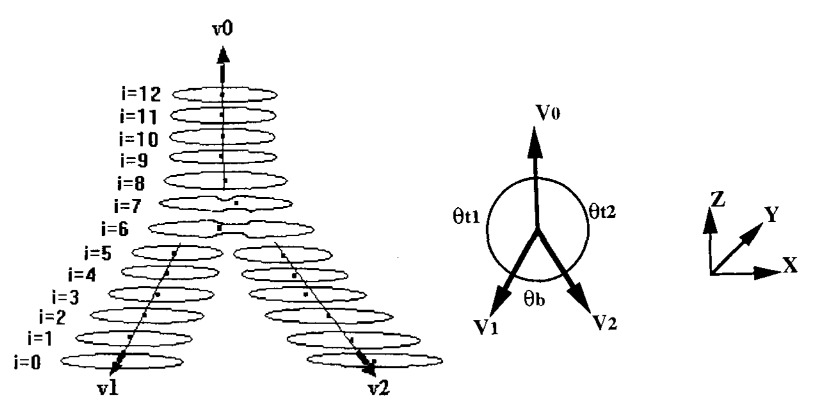

FIGURE 4. An example of the vessel axes at the aortic bifurcation. Slices 6 and 7 are not used to define the axes.

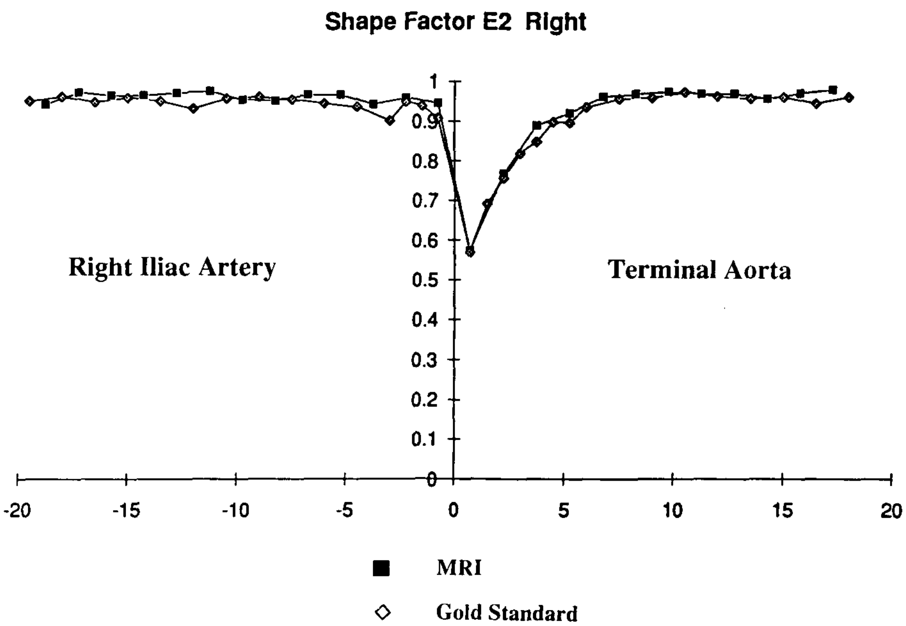

FIGURE 5. Comparison of the shape factors of MR data and the corresponding gold standard.

Human Studies

The *in vivo* studies used the same 3-D TOF MR angiography protocols as those employed for the compliant casts. Institutional Review Board approval was obtained for all investigations on human subjects. Informed consent was obtained from each volunteer prior to the study. A number of selected slice images from the 3-D TOF image set were transferred to the DECstation and used to reconstruct the aortic bifurcation axes and to calculate the branch angles and other geometric parameters using the procedures described earlier.

A preliminary *in vivo* study was carried out in which the reliability and the reproducibility of branch angle measurement were assessed by MR scanning six healthy individuals and measuring their bifurcation angles twice over a one-month period. These six volunteers were selected randomly and without regard to their gender, race, and age. There were four females and two males included in this study. In the absence of any knowledge regarding factors that might affect aortic bifurcation geometry, we standardized the experimental procedure and measured some variables that could conceivably be important. Each volunteer was asked to urinate before MR scanning; no eating was allowed within 2 hr prior to scanning. The two scans of each female were done at approximately the same date during her menstrual cycle. Blood pressure was measured either right before or right after MR scanning.

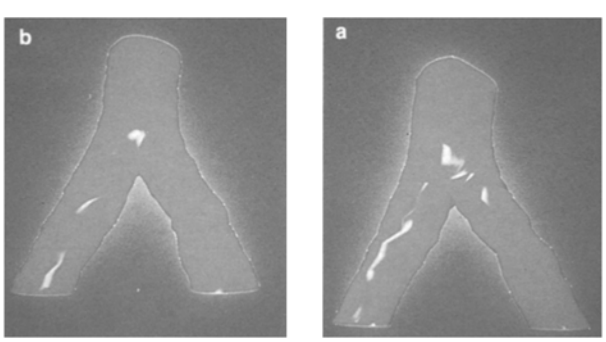

FIGURE 6. 3-D surface rendering of an aortic bifurcation, reconstructed from the MRI images of its compliant replica (right) and the gold standard video data (left). These renderings were obtained using a ray tracing program, RayShade.

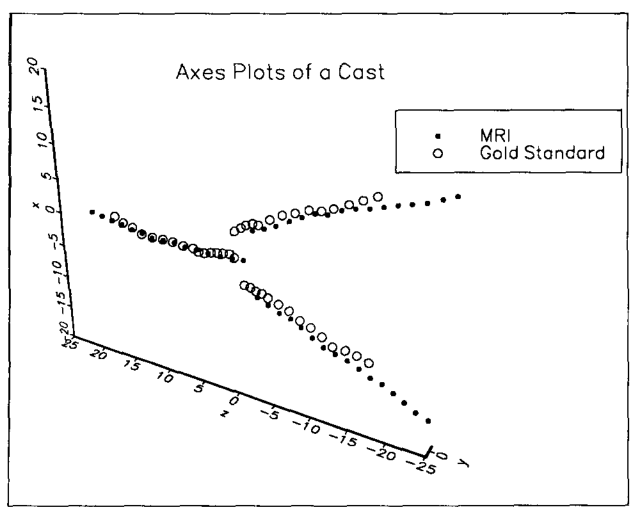

FIGURE 7. 3-D plots of the vessel axes constructed from the centroids of both the MR images of the compliant cast and the video images of the gold standard block.

TABLE 1. Angles and planarity measurements for the three casts.

Cast	Measurement	Bifurcation Angle (degree)	Left Turning Angle (degree)	Right Turning Angle (degree)	Bifurcation Planarity
1	MRI	31.1	160.7	168.2	0.9998
	Gold Standard	31.9	162.2	164.2	0.9952
	difference	−0.8	−1.5	4.0	0.0046
2	MRI	53.8	154.9	150.9	0.9989
	Gold Standard	53.3	153.0	151.8	0.9948
	difference	0.5	1.9	−0.9	0.0041
3	MRI	51.5	134.7	171.3	0.9929
	Gold Standard	50.2	133.7	173.6	0.9928
	difference	1.3	1.0	−2.3	0.0001

Next, the approach was applied to 20 healthy human beings from two age groups. Ten of them were between 56 and 69 years old, and the other 10 were between 21 and 33 years old. In each group, there were 5 males and 5 females and 5 whites and 5 Asians. Ten "matched" pairs were made between the two age groups in order to reduce the confounding effects of race and gender. Using the procedures described earlier, the angles and the other geometric parameters of the aortic bifurcation of each subject were calculated on the workstation. The results from the two age groups were compared statistically using the statistical package, SAS (Cary, NC).

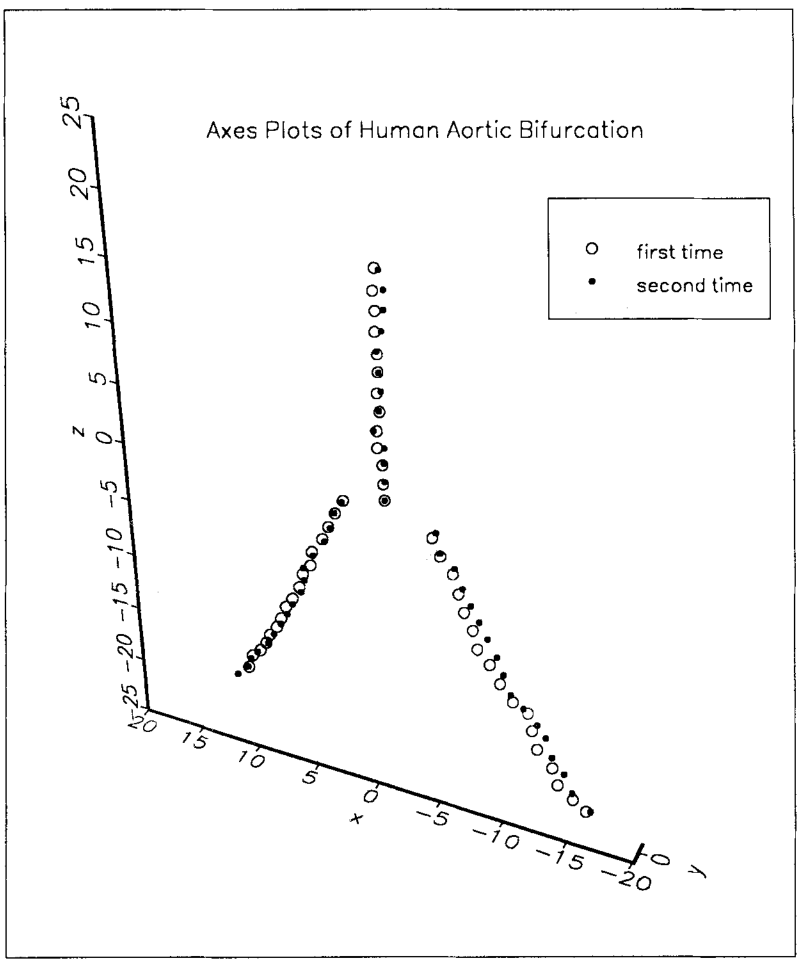

FIGURE 8. 3-D plot of the vessel axes from the first measurement on one subject, superimposed on those from the second measurement.

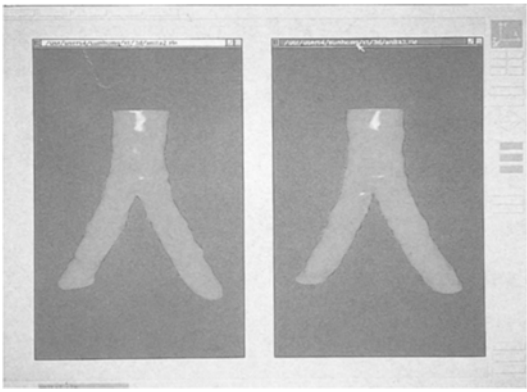

FIGURE 9. Surface reconstructions of the aortic bifurcation from the two MR image sets of one person; the results from the first set are on the left, the second on the right.

RESULTS

Validation of MR Image Analysis

The perimeter, area, and shape factor of individual cross-sections were calculated for both the MR images of the compliant casts and the video images of the corresponding "gold standard" blocks. It was found that the perimeters and the areas were usually larger for the MR images, but a good correlation was found for the shape factors (Fig. 5). This is because the fuzzy boundary of the MR images makes the lumen appear to be larger than it actually is, and the manual outlines are consistently placed at the outer edge of this fuzzy boundary. Both perimeter and lumen area of the MR image are enlarged this way, and the errors cancel out in the definition of the shape factor.

The surface and the axes of the vessels were reconstructed from the MRI contour data. The cross-sectional video images of each of the "gold standard" blocks were also used to construct the vessel surface and axes. The RayShade images (RLE) of one of the bifurcations obtained from the corresponding MRI and gold standard datasets are shown in Fig. 6. These suggest the similarity of the aortic bifurcation geometries reconstructed from the two sets of cross-sectional data. A 3-D plot of the vessel axes from the MR data of one case is superimposed on those from the video images in Fig. 7, which shows a close match between the two.

The bifurcation angle, the left and right turning angles, and the planarity were calculated for the three cases. The results are summarized in Table 1. The differences between the angles obtained from the compliant casts and the blocks were all less than 4°, with a mean error of 0.4° and a standard deviation of 1.9°, which is much less than the normal range of variation of branch angle in the population (2). A paired t-test indicated that there was no statistically significant difference between the angles obtained from the two techniques.

Human Studies

Reproducibility of In Vivo Bifurcation Angle Measurements. The abdominal aortas of six randomly selected healthy individuals were imaged using the 3-D TOF tech-

TABLE 2. Two measurements of the branch angle, the turning angles, and the planarity of the abdominal aortic bifurcation of six normal individuals.

Case	Measurement	Bifurcation Angle (degree)	Left Turning Angle (degree)	Right Turning Angle (degree)	Bifurcation Planarity
1	first	43.2	160.2	154.5	0.9942
	second	42.4	159.0	156.8	0.9943
	difference	0.8	1.2	−2.3	−0.0001
2	first	45.5	156.5	155.6	0.9936
	second	45.0	155.6	156.7	0.9926
	difference	0.5	0.9	−1.1	0.0010
3	first	13.6	177.5	158.7	0.9716
	second	12.1	174.3	159.6	0.9611
	difference	1.5	3.2	−0.9	0.0105
4	first	42.1	160.3	156.4	0.9966
	second	40.0	160.1	159.4	0.9987
	difference	2.1	0.2	−3.0	−0.0021
5	first	31.5	164.4	161.8	0.9937
	second	30.5	164.7	160.0	0.9957
	difference	1.0	−0.3	1.8	−0.0020
6	first	23.2	165.7	170.0	0.9970
	second	23.2	165.3	170.5	0.9972
	difference	0.0	0.4	−0.5	−0.0002

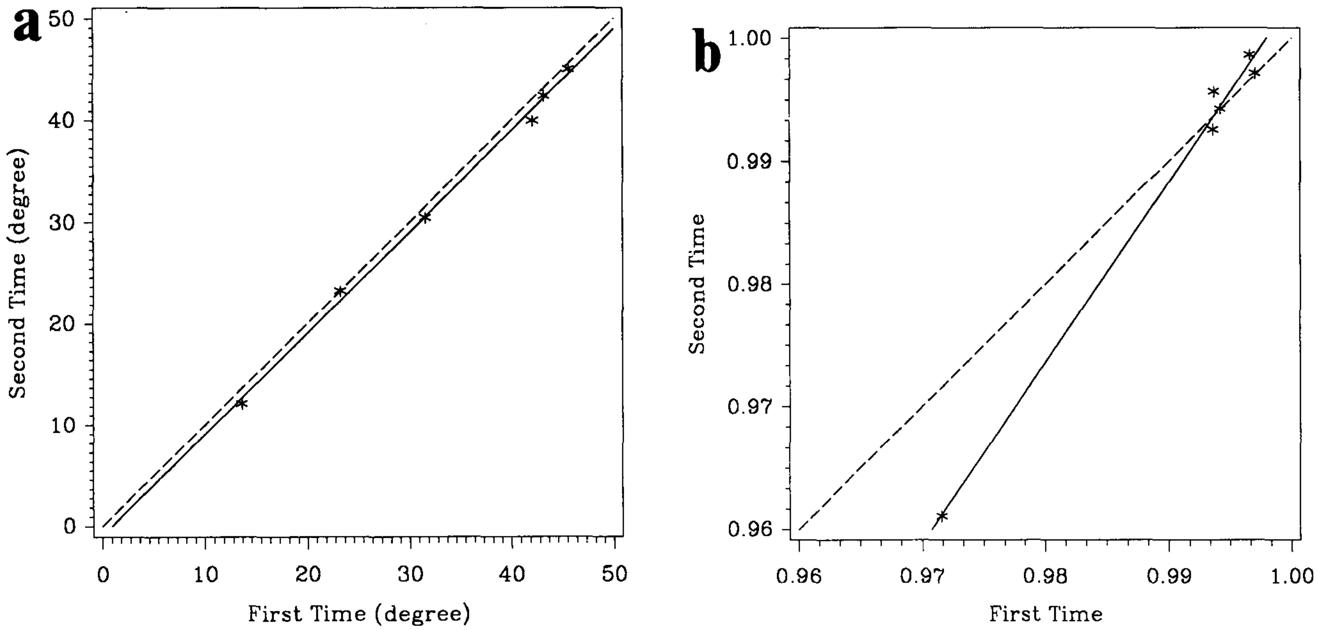

FIGURE 10. Reproducibility of (a) the *in vivo* aortic bifurcation angle measurement and (b) the *in vivo* planarity measurement: the second measurement *vs.* the first measurement. The solid line indicates the linear regression of the two measurements and the dashed line is an identity line.

nique twice over a 1-month period. A 3-D plot of the vessel axes from the first measurement on one subject is superimposed on that from the second measurement in Fig. 8. A close match is seen between the two plots. Figure 9 displays the two surface reconstructions of the aortic bifurcation from two sets of MR images of the same person. The similarity of the vessel shape also suggests the reproducibility of this technique. The six individuals' bifurcation angles, turning angles, and planarities were calculated and are presented in Table 2.

A quantitative comparison was made between the two sets of measurements. For the bifurcation angle, the second measurement differed algebraically from the first measurement by an average of 1.0°, with a standard deviation of the difference of 0.7°. In Fig. 10 (a), the bifurcation angles measured the second time are plotted against the angles measured the first time. Although a paired t-test supported the hypothesis that the second measurement of the bifurcation angle was different from the first measurement (because the second measurement was consistently lower than the first), a strong correlation was obtained for the linear regression in the figure: the correlation coefficient was 0.9983 ($P < 0.0001$).

A similar plot is presented for the planarity measurements in Fig. 10 (b). Again, a highly significant correlation was seen, with $r = 0.9964$ and $P < 0.0001$. The

TABLE 3. The mean and standard deviation of the angles and the planarity at the aortic bifurcation of 20 normal individuals. (N = 10 for each subgroup. NS means $P > 0.1$).

Group	Bifurcation Angle (degree)	Left Turning Angle (degree)	Right Turning Angle (degree)	Angular Asymmetry (degree)	Bifurcation Planarity
All	37.7 ± 10.2	156.3 ± 7.5	158.5 ± 5.2	7.5 ± 7.3	0.979 ± 0.024
Age 56–69	32.8 ± 11.8	154.5 ± 10.0	160.5 ± 5.9	11.2 ± 8.8	0.966 ± 0.029
Age 21–33	42.6 ± 5.1	158.1 ± 3.4	156.4 ± 3.5	3.9 ± 2.5	0.992 ± 0.006
	$P < 0.015$	NS	NS	$P < 0.01$	$P < 0.1$
Males	36.9 ± 12.4	156.3 ± 10.4	157.5 ± 6.2	10.5 ± 8.9	0.975 ± 0.027
Females	38.4 ± 8.0	156.4 ± 3.1	159.5 ± 4.0	4.6 ± 3.8	0.984 ± 0.022
	NS	NS	NS	$P < 0.05$	NS
Asians	41.5 ± 5.2	155.6 ± 4.5	158.4 ± 4.6	5.5 ± 5.3	0.987 ± 0.010
Whites	33.8 ± 12.6	157.1 ± 9.8	158.5 ± 5.9	9.6 ± 8.7	0.971 ± 0.032
	$P < 0.05$	NS	NS	NS	NS

mean algebraic difference of the paired measurements was 0.0012 and the standard deviation of the difference was 0.0047. A paired t-test indicated that the two measurements on each subject were equal at the 0.05 significance level.

These results show that the MR technique for *in vivo* vascular geometry measurement is reproducible and that the geometry of the human abdominal aortic bifurcation normally does not change within a short period of time. Therefore, single measurements of geometric parameters based on MR data are reliable.

The Geometry of the Human Aortic Bifurcation. The bifurcation angle and the two turning angles were measured from the MR images of 20 normal individuals in two age groups as described in the Methods. The planarity and the angularity asymmetry of the bifurcation were also calculated for the 20 volunteers. The bifurcation angle ranged from 12.1 to 50.3, the angular asymmetry ranged from 0.7 to 31.4, and the bifurcation planarity ranged from 0.9060 to 0.9987. The means and the standard deviations of the geometric parameters are summarized in Table 3.

One-sided two-sample t-tests were applied to the data. The results suggest that older people have a smaller bifurcation angle and planarity but larger angular asymmetry than young people. Statistics for the two gender groups showed that the angular asymmetries were significantly different for males and females. This result is similar to those reported earlier (2). To our knowledge, no work has been reported comparing the geometry of the human aortic bifurcation among different races. The differences in the angular asymmetry and the planarity of the aortic bifurcation between Asian and whites are not statistically significant, but there is a significant difference for the aortic bifurcation angle. In assessing the quantitative significance of these statistical tests, it should be noted that the study population was selected in such a way that it is likely that the geometric variables in each subpopulation were not normally distributed.

The above statistical analyses were done for each demographic that the geometric variables in each subpopulation were not normally distributed, factor (age, race, and gender) separately. A general linear models procedure was applied to perform an analysis of covariance on a model containing all three factors. The results show that age has an effect on the branch angle ($P < 0.05$), the angular asymmetry ($P < 0.02$), and the planarity of the bifurcation ($P < 0.01$). Race has an effect on the branch angle at a given age ($P < 0.1$). Gender has an effect on the angular asymmetry at a given age ($P < 0.09$). There is no significant effect of race or gender on the relationship between branch angle and age, planarity and age, or angular asymmetry and age. This is consistent with the results of the t-tests reported in Table 3.

DISCUSSION

In this paper, a computer modeling approach has been developed to measure the geometric parameters at arterial bifurcations, such as the bifurcation angle, the turning angles, the angular asymmetry, and the planarity of the bifurcation, based on MR angiographic imaging.

The reconstruction process begins with the extraction of the coordinate points of the vessel contours from 2-D cross-sectional MR images. Manual segmentation, used in this pilot study, is a time-consuming task. In recent years, there has been considerable research on automatic segmentation algorithms for tomographic data (12). Since MR datasets are extremely complicated, user interaction may never become entirely redundant. It may be reduced by the use of appropriate algorithms (*e.g.*, region growing, edge detection, thresholding, classification, and others) and graphical editing functions. The robustness of the segmentation may be increased by using these semi-automatic methods. But the goal of a fully automatic segmentation system is not likely to be reached without the introduction of artificial intelligence methods.

The estimates of the angles at the bifurcation were made after the centroids of the vessel cross-sections had been determined by averaging the coordinates of the vessel boundary points; the centroids were then connected to obtain the 3-D vessel axes. The angles were used to calculate the planarity of the bifurcation. These algorithms were applied to both the MRI data obtained from three compliant bifurcation casts which were made with Sylgard silicone rubber, and the video image data obtained from "gold standard" rigid plastic blocks which reproduced the interior shape of the compliant casts. A good correlation was found between the shape factors and bifurcation angles obtained from the MR images of the compliant casts and from the video images of the milled "gold standard" rigid blocks. The 3-D reconstructions of the vessel interior surface and the vessel axes from the two sets of data are also very similar. The results indicate the accuracy of geometric measurements based on the MR technique.

The reliability of this approach was also examined in human studies. The preliminary tests indicated that the geometry of the human abdominal aortic bifurcation normally does not change within a short period of time. The reproducibility of the technique, seen in the human studies, and the success of the *in vitro* validation experiments, suggest that single measurements of *in vivo* geometric parameters based on MRI data are reliable.

In subsequent human studies, MR images of a small population of normal individuals were used to examine the variability of the geometry of the human aortic bifurcation. It can be seen clearly that the bifurcation angle, the angular asymmetry, and the planarity of the bifurcation vary from one person to another, and the ranges of variation are larger for older people than for younger people. Differences between subgroups are also evident.

The lack of homogeneity among the samples undoubtedly contributed to the variability of the bifurcation geometry within the subgroups, thus making differences between them harder to detect. With respect to age effects, it might be ideal to follow the bifurcation angle and other geometric parameters of a selection of individuals over time, to eliminate additional sources of variability, but this experiment is not realistic.

Since the sample size and the power of comparison tests (or the probability of type II error) are closely connected, a specified difference in means is easier to detect for larger sample sizes than for smaller ones. The required sample size is also determined by the variance or the standard deviation of the measured quantity. For example, to detect a 10° difference in the bifurcation angle when its standard deviation is 10°, a sample size of 17 for each group is required to obtain a 0.80 power at the 0.05 significance level (18).

Despite the considerable scatter in the measurements, it is seen that the geometry of the aortic bifurcation is related to age, gender, and race. It was reported in the earlier literature that no significant correlation was found between the branch angle, angular asymmetry, and flow divider offset of the aortic bifurcation and age (2,16). But our results show that older people tend to have a smaller bifurcation angle, lower planarity, and larger angular asymmetry than younger people. Asians have larger bifurcation angles than whites at a given age. The bifurcation of males is more asymmetric than that of females, which is similar to those reported earlier (2). Larger samples will be necessary to draw more quantitative conclusions about the size of these differences in the geometry of the human aortic bifurcation.

These results suggest that it may be possible to examine, in a selected population, the relationship between pathologic conditions at arterial bifurcations and the geometric parameters of the branch. Connections might be sought between "suboptimal" branching and vascular disease.

REFERENCES

1. Appel, A. Some techniques for shading machine renderings of solids. AFIPS 1968 Spring Joint Comput. Conf. 37–45; 1968.
2. Bargeron, C.B.; Hutchins, G.M.; Moore, G.W.; Deters, O.J.; Mark, F.F.; Friedman, M.H. Distribution of the geometric parameters of human aortic bifurcations. Arteriosclerosis 6:109–113; 1986.
3. Chakeres, D.W.; Schmalbrock, P. Fundamentals of magnetic resonance imaging. Baltimore: Williams & Wilkins; 1992.
4. Christiansen, H.N.; Sederberg, T.W. Conversion of complex contour line definitions into polygonal element mosaics. Comput. Graph. 12:187–192; 1978.
5. Edelman, R.R.; Mattle, H.P.; Atkinson, D.J.; Hoogewoud, H.M. MR angiography. Am. J. Radiology 154:937–946; 1990.
6. Fanucci, E.; Orlacchio, A.; Pocek, M. The vascular geometry of human arterial bifurcation. Investigative Radiology 23:713–718; 1988.
7. Fessler, J.A.; Macovski, A. Object-based 3-D reconstruction of arterial trees from magnetic resonance angiograms. IEEE Trans. Med. Imaging 10:25–39; 1991.
8. Friedman, M.H.; Deters, O.J.; Mark, F.F.; Bargeron, C.B.; Hutchins, G.M. Arterial geometry affects hemodynamics. A potential risk factor for atherosclerosis. Atherosclerosis 46:225–231; 1983.
9. Friedman, M.H.; Hacker, V.A.; James, B.F.; Kuban, B.D.; Qin, J.; Schmalbrock, P. MRI measurement of arterial branch geometry. In: Spilker, R.L.; Friedman, M.H., eds. 1991 Biomechanics Symposium. ASME 120:45–48; 1991.
10. Friedman, M.H.; O'Brien, V.; Ehrlich, L.W. Calculation of pulsatile flow through a branch—Implications for the hemodynamics of atherogenesis. Circulation Research 36:277–285; 1975.
11. Geckle, W.J.; Friedman, M.H. 3-D reconstruction of coronary artery medial axes from bi-plane angiography. IEEE Computers in Cardiology 269–273; 1978.

14. Jackson, T.; Merickel, M.; Spetz, K. Segmentation of the abdominal aorta from transverse MR images. Annual International Conference of the IEEE Engineering in Medicine and Biology Society 12:183–184; 1990.

13. Keller, P.J.; Drayer, B.P.; Fram, E.K.; Williams, K.D.; Dumoulin, C.L.; Souza, S.P. MR angiography with two-dimensional acquisition and three-dimensional display. Radiology 173:527–532; 1989.

14. Keller, P.J. Time-of-Flight Magnetic Resonance Angiography. In: Keller, P.J.; Drayer, B.P.; Fram, E.K., eds. Neuronimaging Clinics of North America. W.B. Saunders Company 2:639–656; 1992.
15. Kuban, B.D.; Friedman, M.H. The effect of pulsatile frequency on wall shear in a compliant cast of a human aortic bifurcation. In: Vanderby, R., ed. Advances in Bioengineering. ASME, New York: 13–16, 1991.
16. Lee, Y.N.; Keitzer, W.F.; Watson, F.R.; Liu, H. Vascular geometry at the abdominal aortic bifurcation. JAMWA 37: 77–81; 1982.
17. Lim, T.H.; Saloner, D.; Anderson, C.M. Current applications of magnetic resonance vascular imaging. Cardiac Imaging 7:661–680; 1989.
18. Montgomery, D.C. Design and analysis of experiments. 3rd edition. John Wiley & Sons, Inc., 1991.
19. Osbakken, M. Vascular anatomy and physiology studied with MRI techniques. In: Osbakken, M.; Haselgrove, J., eds. NMR techniques in the study of cardiovascular structure and function. Mount Kisco, New York: Futura Publishing Company, Inc., 1988: pp. 81–93.
20. Peifer, J.W.; Ku, D.N. Visualization of the abdominal aorta using three-dimensional computer models reconstructed from MR images. IEEE Proc. First Conf. Visualization Biomed. Comput. 252–257; 1990.
21. Raso, A.M.; Levis, P.; Sottimano, C. Geometry of aortoiliac bifurcation in healthy men and women as possible atherogenetic risk factors. Panminerva Medica 23:33–37; 1981.
22. Rossnick, S.; Kennedy, D.; Laub, G.; Nelson, A.;

Braeckle, G.; Dzik, A.; Bachus, R.; Starewicz, P. Three dimensional display of blood vessel in MRI. Computer in Cardiology IEEE 193–196; 1986.
23. Saltissi, S.; Webb-Peploe, M.M.; Coltart, D.J. Effect of variation in coronary artery anatomy on distribution of stenotic lesions. British Heart Journal 42:186–191; 1979.
24. Sharp, W.V.; Donovan, D.L.; Teague, P.C.; Mosteller, R.D. Arterial occlusive disease: a function of vessel bifurcation angle. Surgery 91:680–685; 1982.
25. Schmalbrock, P.; Yuan, C.; Chakeres, D.W.; Kohli, J.; Pelc, N.J. Volume MR angiography: Methods to achieve very short echo times. Radiology 175:861–865; 1990.
26. Smith, M.A. The measurement and visualization of vessel blood flow by magnetic resonance imaging. Clin. Phys. Physiol. Meas. 11:101–123; 1990.
27. Spickler, E.; McKenna, K.M.; Lufkin, R.B. Approaches to MR angiography. Comp. Med. Imag. and Graphics 12:211–217; 1988.
28. Uyama, C.; Akutsu, T. Three-dimensional interface geometry of the human heart with the artificial heart. Trans. Am. Soc. Artif. Intern. Organs 37:608–614; 1991.
29. Vesely, I.; Eickmeier, B.; Campbell, G. Automated 3-D reconstruction of vascular structures from high definition casts. IEEE Trans. Biomed. Eng. 38:1123–1129; 1991.
30. Wrazidlo, W.; Brambs, H.J.; Lederer, W.; Schneider, S.; Geiger, B.; Fischer, C. An alternative method of three-dimensional reconstruction from two-dimensional CT and MR data sets. European Journal of Radiology 12:11–16; 1991.